ResearchGate

See discussions, stats, and author profiles for this publication at: https://www.researchgate.net/publication/239633533

Evidence of Matrix Lattice Distortion in Zn 1− x Co x O Nanocrystals

ARTICLE *in* THE JOURNAL OF PHYSICAL CHEMISTRY C · MARCH 2009

Impact Factor: 4.77 · DOI: 10.1021/jp807459s

CITATIONS
6

READS
17

9 AUTHORS, INCLUDING:

Shuo Zhang
Toulouse Business School
109 PUBLICATIONS **1,008** CITATIONS
SEE PROFILE

W. S. Chu
University of Science and Technology of C…
105 PUBLICATIONS **767** CITATIONS
SEE PROFILE

Wensheng Yan
University of Science and Technology of C…
79 PUBLICATIONS **1,070** CITATIONS
SEE PROFILE

Available from: W. S. Chu
Retrieved on: 01 February 2016

THE JOURNAL OF PHYSICAL CHEMISTRY C

Subscriber access provided by INST OF HIGH ENERGY PHYSICS

Article

Evidence of Matrix Lattice Distortion in ZnCoO Nanocrystals

Shuo Zhang, Yaping Du, Haiming Li, Wangsheng Chu, Jiong Li, Wensheng Yan, Shiqiang Wei, Chunhua Yan, and Ziyu Wu

J. Phys. Chem. C, **2009**, 113 (11), 4263-4269• DOI: 10.1021/jp807459s • Publication Date (Web): 20 February 2009

Downloaded from http://pubs.acs.org on March 12, 2009

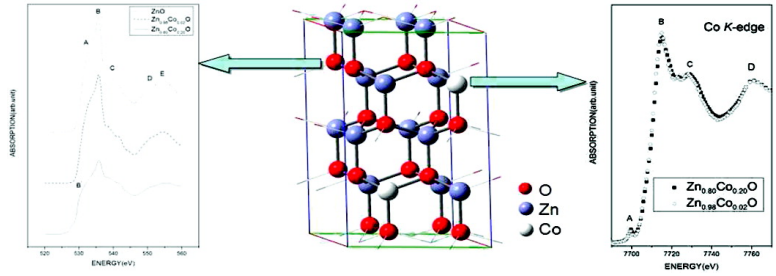

More About This Article

Additional resources and features associated with this article are available within the HTML version:

- Supporting Information
- Access to high resolution figures
- Links to articles and content related to this article
- Copyright permission to reproduce figures and/or text from this article

View the Full Text HTML

ACS Publications
High quality. High impact.

The Journal of Physical Chemistry C is published by the American Chemical Society. 1155 Sixteenth Street N.W., Washington, DC 20036

ARTICLES

Evidence of Matrix Lattice Distortion in $Zn_{1-x}Co_xO$ Nanocrystals

Shuo Zhang,[†,‡] Yaping Du,[§] Haiming Li,[†] Wangsheng Chu,*[,†] Jiong Li,[†] Wensheng Yan,[‡] Shiqiang Wei,[‡] Chunhua Yan,[§] and Ziyu Wu*[,†,‡,∥]

Beijing Synchrotron Radiation Facility, Institute of High Energy Physics, Chinese Academy of Sciences, Beijing 100049, China, National Synchrotron Radiation Laboratory, University of Science and Technology of China, Hefei, Anhui 230029, China, Beijing National Laboratory of Molecular Science, State Key Laboratory of Rare Earth Materials Chemistry and Applications, PKU-UKU Joint Laboratory in Rare Earth Materials and Bio-Inorganic Chemistry, Peking University, Beijing 100871, China, and Theoretical Physics Center for Science Facilities, Chinese Academy of Sciences, Beijing 100049, China

Received: August 20, 2008; Revised Manuscript Received: December 12, 2008

In this work, we investigated the doping effect on the local structure of Co, Zn, and O in $Zn_{1-x}Co_xO$ (x = 0.02 and 0.2) nanocrystals by X-ray absorption spectroscopy combined with ab initio calculations. We identified the presence of a distorted CoO_4 structure and showed that the distortion propagates homogeneously in the matrix with increasing doping concentration. The presence of a distorted matrix lattice plays an important role in the mechanism of room-temperature ferromagnetism observed in diluted magnetic semiconductor materials, which is in agreement with a new mechanism recently introduced. Information on the electronic structure of the bottom of the conduction band has been achieved by O K-edge X-ray absorption near-edge spectroscopy that also addresses significant contributions of the matrix lattice distortion on the distribution of O 2p states.

Introduction

In the past decade, following the first report by Ohno,[1] diluted magnetic semiconductor (DMS) materials attracted considerable interest because of their potential promising applications in spintronic devices.[2] However, the understanding of this new class of materials is a real challenge because of their anomalous magnetic behavior and the occurrence of room-temperature ferromagnetism (RTF). Several manuscripts are available in the literature, and some controversial interpretations have been proposed.[3−7] Some interpretations addressed the RTF origin to the presence of magnetic clusters or secondary phases,[3,4] while others associated the observed RTF to intrinsic properties of the systems.[5−7] At the same time, a consensus exists on the presence in these materials of a conventional superexchange or a double-exchange interaction, i.e., a mechanism that does not support the existence of long-range magnetic order at concentrations of magnetic cations of a few percent. Several theoretical frameworks capable of treating this fundamental aspect have also been proposed. Dietl et al. calculated the Curie temperature for various p-type semiconductors by means of the Zener model. They suggested that both ZnO and GaN are suitable DMS materials, and RTF is possibly due to the interplay of magnetic ion doping with the hole content in the host semiconductor.[8] RTF behavior in insulators can be also explained, as proposed by Coey et al., via a ferromagnetic exchange mechanism mediated by shallow donor electrons forming bound magnetic polarons (BMPs).[9] In particular, spin−orbit lattice coupling has been used to introduce a new mechanism that considers the magnetoelastic effect of $3d^n$ ions with Jahn−Teller orbital occupancy as the origin of the lattice-assisted spin ordering.[10] In this framework, a previous experimental investigation[11] can be reasonably understood.

Material properties are in a close relationship with its atomic structure, so investigations of the local structure around magnetic ions are important for clarifying anomalous behaviors. To this purpose, extended X-ray absorption fine structure (EXAFS) and X-ray absorption near-edge spectroscopy (XANES) experiments[12−15] on Co-doped ZnO compounds have been performed in order to characterize the environment around magnetic ions, e.g., bond lengths, coordination numbers, and site symmetry. Moreover, a few investigations addressed the possible role of the distortion of the matrix structure to the RTF mechanism, and actually, there is still a lack of systematic investigations of the local structure of the host atoms.

In this paper, we report a systematic study of the doping effect on local structures around Co, Zn, and O and of the electronic structure of the bottom of the conduction band in $Zn_{1-x}Co_xO$ (x = 0.02 and 0.2) nanocrystals by using X-ray absorption spectroscopy (XAS) combined with ab initio calculations. EXAFS and XANES experimental methods are powerful probes in investigating local and electronic structures[16] and multiple-scattering (MS) calculations are very useful in interpreting XANES spectral features. Moreover, at the O K-edge, because of the occurrence of strong hybridization mechanisms and because of the small oxygen 1s core-hole lifetime broadening

* Authors to whom correspondence should be addressed. E-mail: wuzy@ustc.ac.cn (Z.W.) and cws@ihep.ac.cn (W.C.).
[†] Institute of High Energy Physics, Chinese Academy of Sciences.
[‡] University of Science and Technology of China.
[§] Peking University.
[∥] Theoretical Physics Center for Science Facilities, Chinese Academy of Sciences.

10.1021/jp807459s CCC: $40.75 © 2009 American Chemical Society
Published on Web 02/20/2009

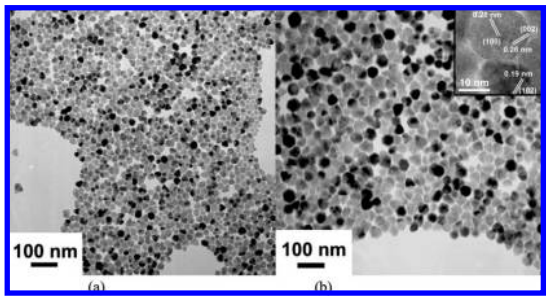

Figure 1. TEM images of $Zn_{1-x}Co_xO$ samples. Photographs (a) and (b) refer to 2% and 20% concentrations, respectively. The inset of panel b shows a HRTEM image of the $Zn_{0.8}Co_{0.2}O$ sample. TEM images reveal monodispersed ZnO:Co nanocrystals, mainly composed of dot-shaped nanocrystals. The sample crystallite size is 32.2 ± 4.3 nm for ZnO/2% Co and 56.6 ± 5.2 nm for ZnO/20% Co. The clear-cut lattice fringes appearing in the HRTEM image confirm the high crystallinity of both ZnO and Co nanocrystals. Interplanar spacings at 0.26, 0.28, and 0.19 nm are assigned to the (002), (100), and (102) planes of the wurtzite ZnO crystal structure, respectively.

in respect to the corresponding transition metal (TM) 1s core-hole lifetime, the analysis of the edge features may return accurate electronic information not available from the corresponding transition metal K-edge data.

Experiments and Sample Preparation

Next, we will summarize the synthesis of $Zn_{1-x}Co_xO$ ($x = 0.02$ and 0.2) nanocrystalline samples with different Co doping concentrations. More information is available in ref 17. Acetylacetonates were employed as precursors. For a typical synthesis, we started from $Zn_{0.98}Co_{0.02}O$ using stoichiometric zinc acetylacetonates (1.33 mmol) and cobalt acetylacetonates (0.065 mmol) dissolved in a three-neck round-bottomed flask with 10.5 mL of oleyamine (80−90%, Acros Organics) and 10.5 mL of 1-octadecene (90%, Acros Organics) (v:v, 1:1). The flask was fit in a condenser and heated to 373 K to remove water and oxygen with vigorous magnetic stirring under vacuum for 20 min in a temperature-controlled electromantle. Then, under air atmosphere, the solution was heated to 583 K at a rate of 20 K/min and then left at high temperature for 60 min. After that, the solution was cooled to room temperature, and nanocrystals were precipitated with the addition of excess ethanol. The products were washed with excess ethanol several times and dried in air at 60 °C for 3 h. The as-prepared nanocrystals were easily dispersed in nonpolar organic solvents (e.g., cyclohexane or hexane). Sample morphologies were characterized with a transmission electron microscope (TEM 200CX JEOL) at 160 kV (Figure 1) and with a high-resolution transmission electron microscope (HRTEM H-9000 Hitachi) at 300 kV.

Co and Zn K-edge XAS spectra of $Zn_xCo_{1-x}O$ powders were measured at beamline 1W1B at the Beijing Synchrotron Radiation Facility (BSRF). For the Co K-edge XAS, the lower-concentration sample was measured in fluorescence, while the higher-concentration sample was measured in transmission. For the Zn K-edge XAS, both measurements were performed in transmission mode. The electron beam energy of the storage ring was 2.2 GeV, and the maximum stored current was about 200 mA. Data were recorded using a Si(111) double crystal monochromator. For the Co K-edge, in the energy range selected for the experiments, a detuning of 30% between silicon crystals was performed to suppress the high harmonics content. The O K-edge XANES spectra were measured at beamline U19 at the Chinese National Synchrotron Radiation Laboratory (NSRL) at Hefei. The radiation collected by a bending magnet was monochromatized with a varied line-spacing plane grating and refocused on the sample by a toroidal mirror. Experiments were performed with a resolution of about 0.2 eV, and spectra were collected in the total electron yield mode working in a HV chamber at a vacuum pressure of $<5 \times 10^{-7}$ Pa.

Calculations

XANES has been performed in the framework of the multiple-scattering (MS) theory[18,19] using the FEFF 8.2 code.[20] Co K-edge XANES calculations were performed with the structure model and lattice parameters of the host structure, i.e., wurtzite ZnO, in which Zn is replaced by a Co atom as the absorber. The FEFF input file was generated by the ATOMS package for lattice constants $a = 3.242$ Å, $b = 3.242$ Å, and $c = 5.206$ Å. The cluster potential was approximated by a set of spherically averaged muffin-tin (MT) potentials. For the calculations, we used the Hedin-Lundqvist model.[19,21] A model cluster size up to 126 atoms was used in all MS calculations to obtain accurate self-consistent field (SCF) calculations, and a cluster of 177 atoms was used for full multiple-scattering calculations. A similar framework for the O K-edge XANES calculations has also been considered.

For EXAFS data fitting, theoretical curves were carried out by ab initio modeling with the FEFF 8.2 code (Supporting Information). The backscattering amplitudes and total phase shifts were calculated using the same wurtzite ZnO model cluster. The IFEFFIT[22] program was used to fit spectra in the R space in the range of 1−3 Å, including the first and second coordination shells. The E_0 and the overall amplitude factor S_0^2 were obtained by fitting the reference ZnO EXAFS data. Bond lengths and Debye−Waller factors (σ^2) of the different shells were left as free parameters, while the numbers of neighbors were fixed to crystallographic values of the reference ZnO system.

Density of states (DOS) calculations were performed using the density functional theory (DFT) as implemented in the Vienna ab initio simulation package (VASP).[23] The projector augmented wave was used to describe the electron−ion interaction. The local density approximation (LDA) has been used for the exchange−correlation functional in the pure ZnO system, while LSDA+U, in which U was set to 3.5 eV for 25% doped ZnO, has been used to simulate the $Zn_{0.8}Co_{0.2}O$ sample. A centered $5 \times 5 \times 5$ k mesh was used for Brillouin zone sampling, and the electronic wave function was expanded using plane waves up to a cutoff energy of 500 eV.

Results and Discussion

A. Metal K-edge XANES. Co K-edge XANES spectra of $Zn_{1-x}Co_xO$ have been measured in the energy range of 7692−7738 eV. Data shown in Figure 2a exhibit four main features labeled from A to D. All spectra are very similar and display a weak pre-edge peak (A), a sharp absorption rise to a large narrow peak (B), followed by a second structure (C), and a broader peak (D) at high energy. Because the amplitude of the photoelectron scattering of Zn and Co is much smaller than oxygen, the characteristic shape of the white line (peak B) and thus the energy distribution of the p-like density of states are mainly determined by the type and arrangement of the first-shell neighbors.[24] From Figure 2a, we also recognize that the intensity and shape of peak B are almost independent of cobalt, suggesting a negligible effect of doping for the first coordination shell and for distribution of the Co p-like density of the state of $Zn_{1-x}Co_xO$ nanocrystals.

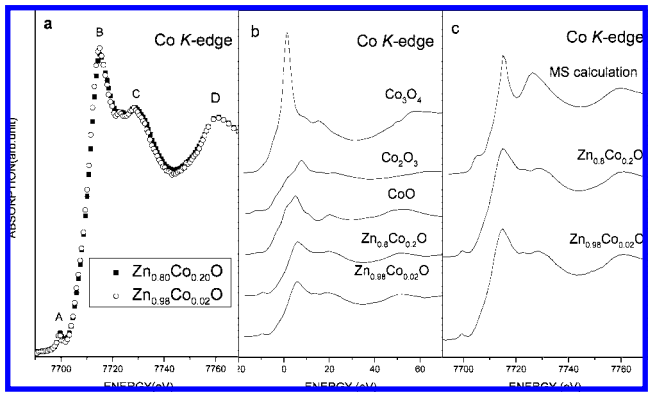

Figure 2. (a) Comparison of Co K-edge XANES spectra of $Zn_{1-x}Co_xO$ ($x = 0.02$ and 0.20) samples. (b) Comparison of Co K-edge XANES spectra of $Zn_{1-x}Co_xO$ and cobalt oxides. (c) Comparison of Co K-edge XANES spectra of $Zn_{1-x}Co_xO$ samples with simulations of Co-doped ZnO.

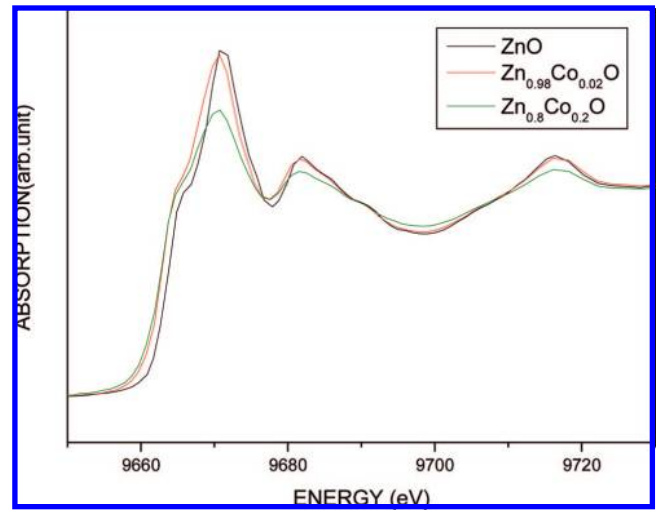

Figure 3. Comparison of Zn K-edge XANES spectra of $Zn_{1-x}Co_xO$ ($x = 0$, 0.02 and 0.20).

Studying the available literature, we find the origin of the pre-edge features at the metal K-edge XANES of transition metal monoxides can be associated with (1) a dipole transition due to the 3d−4p mixing of metal states, (2) a quadrupole transition of a 1s electron to the 3d orbital,[25] or (3) the hybridization between 4p states of the central metal and higher neighboring 3d metal orbitals.[26]

To gain further insight into the local environments around doping ions, we compare XANES spectra of $Zn_{1-x}Co_xO$ systems with cobalt oxides in Figure 2b, aligning spectra to the rising absorption edge. The comparison shows the intensity of the pre-edge peak in the central symmetry of the Co_nO_m clusters such as CoO is very weak. For other asymmetric local structures such as Co_2O_3 or Co_3O_4, the feature is still detectable, but in the oxides its position changes. From Figure 2b, the intensity and position of peak A in the $Zn_{1-x}Co_xO$ systems are different from cobalt oxides, ruling out the possible occurrence of a second phase in these samples. Moreover, the local coordination symmetry of cobalt atoms would be different from that of Co_2O_3 or Co_3O_4 and noncentrosymmetric systems, so that cobalt atoms may actually replace zinc ions in the lattice. To support this latter hypothesis, detailed XANES simulations at the Co K-edge of $Zn_{1-x}Co_xO$ systems have been performed. Calculations shown in Figure 2c are in good agreement with experimental data, demonstrating that cobalt atoms may actually replace Zn-forming CoO_4 tetrahedra. In the case of a tetrahedral environment, the main contribution to the pre-edge feature comes from a dipole-allowed transition from 1s to 3d−4p mixing states.[27] As a consequence, the pre-edge peak in $Zn_{1-x}Co_xO$ appears mainly determined by the arrangement of the first-shell atoms. From Figure 2a, we also noticed negligible changes in peak A between the two samples, addressing the occurrence of a similar magnetic environment almost independent of doping.

To better understand the doping effect on the local structure of the ZnO matrix, we also compared XANES at the Zn K-edge. In Figure 2, we show the comparison of experimental data of the pure ZnO with the 2% and 20% cobalt content samples. Because of the lack of empty Zn 3d states, no pre-edge peak is observed at the Zn K-edge, and attention has to be given to the white line behavior. In Figure 3, we see that the spectrum of $Zn_{0.98}Co_{0.02}O$ is very similar to that of ZnO, while in $Zn_{0.8}Co_{0.2}O$ a broader and lower-intensity white line resonance is observed. Taking into account the data at the Co K-edge, this behavior can be understood when considering a rearrangement of the first oxygen coordination shell. Similar to what has been previously reported[14] and taking into account data for $Zn_{0.98}Co_{0.02}O$, the decrease in intensity implies the presence of distorted ZnO_4 tetrahedra in the $Zn_{0.8}Co_{0.2}O$ system. On the other hand, a broader white line peak also reflects an increase of delocalized states, which is not in agreement with the effective reduction of Zn atoms and the following increase in the localization of Zn 4p states that, on the contrary, could induce sharpening of the resonance. In fact, the observed behavior is probably due to an increase in hybridization among Zn 4p, O 2p, and Co 3d states. The mechanism will be discussed in the section devoted to the analysis of O K-edge XANES. However, from the comparison of XANES spectra at Co and Zn K-edges, we have to stress that the Zn local environment is much more sensitive to doping than the Co local environment. Another important issue in these systems is the surface effect on the local structure because of the nanocrystal characters of these samples. Actually, the presence of a surface area where the lattice is truncated would result in lattice distortion on the surface and near-surface region. However, in the case of our samples, the mean size of the nanocrystals is approximately 35 nm for the 2% doped sample and 60 nm for the 20% doped sample, and XAS data at Co and Zn *K*-edges are mainly bulk sensitive, so that the potential surface effect for our discussion is negligible.

B. EXAFS Data Fitting. Fourier-transform (FT) Co and Zn EXAFS spectra for the two doped concentrations are plotted in panels a and b of Figure 4, while the corresponding $k^2\chi(k)$ functions are shown in the insets. From the Co K-edge data, it can be seen that the overall oscillations of both the $Zn_{0.8}Co_{0.2}O$ and $Zn_{0.98}Co_{0.02}O$ samples are similar to that of the pure ZnO, indicating that Co mostly occupies Zn sites. Actually, the first two intense peaks in the FT data result from a simple backscattering of the photoelectrons from the first coordination shell of four oxygen atoms and the second shell of cations. In the two doped samples, the intensity and position of the first peak of the FT of the Co K-edge coincide, while at the Zn K-edge, the intensities of the peaks of the FT significantly change, and the $Zn_{0.8}Co_{0.2}O$ sample exhibits a lower intensity when compared to the $Zn_{0.98}Co_{0.02}O$ sample.

Data of the EXAFS fits are summarized in Table 1 and show, within experimental accuracy, that the first coordination neighbor distances are almost independent of doping for both Co and Zn. In all samples, the Co−O distance is the same as the Zn−O distance, and this distance is close to that of pure ZnO, clearly supporting the replacement of zinc by cobalt atoms. Doping

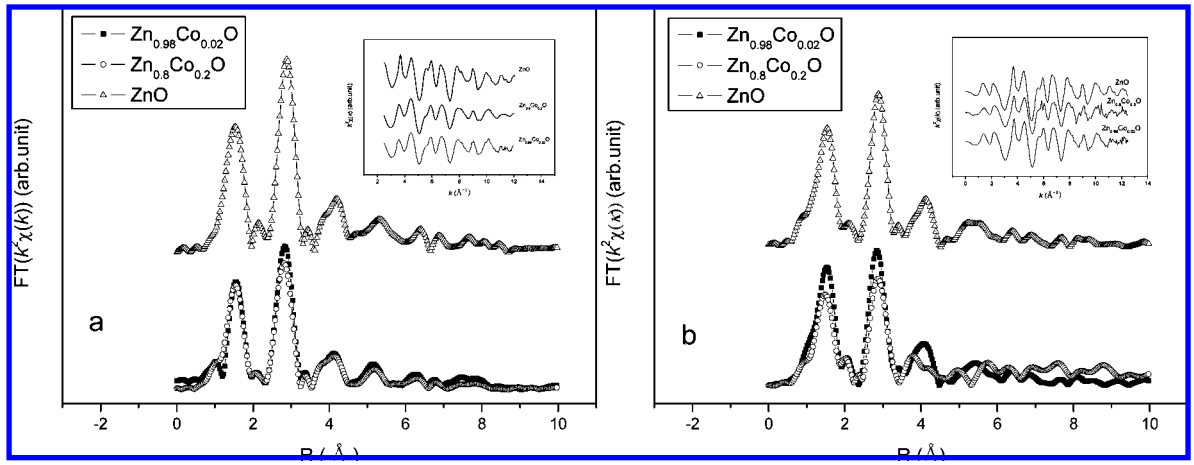

Figure 4. (a) Comparison of the Co K-edge Fourier transforms of the $k^2\chi(k)$ EXAFS signals of $Zn_{1-x}Co_xO$ compounds. (b) Comparison of the Zn K-edge Fourier transforms of the $k^2\chi(k)$ EXAFS signals for $Zn_{1-x}Co_xO$ compounds. Inset shows the corresponding EXAFS $k^2\chi(k)$ functions.

TABLE 1: Parameters of the Fit of the $Zn_{1-x}Co_xO$ ($x = 0$, 0.02, and 0.20) Samples

sample	bond type	N	R (Å)	σ^2 (10^{-3} Å^2)
$Zn_{0.98}Co_{0.02}O$	Co−O	4	1.96 ± 0.01	3.5 ± 1.2
	Zn−O	4	1.96 ± 0.01	2.7 ± 1.3
$Zn_{0.8}Co_{0.2}O$	Co−O	4	1.96 ± 0.01	4.2 ± 0.8
	Zn−O	4	1.95 ± 0.01	5.5 ± 1.0
reference ZnO		4	1.97	−

mechanisms may also be investigated by studying the behavior of the Debye−Waller factor, σ^2. For the first coordination shell, we see that σ^2 increases with doping. This is expected because local structure distortions may occur as a consequence of a lattice mismatch induced at high levels of doping. Moreover, at low doping, the σ^2_{Co-O} is slightly larger than σ^2_{Zn-O}, while the high level of doping of σ^2_{Co-O} is a little smaller than that of σ^2_{Zn-O}. Moreover, almost no changes are detected in σ^2_{Co-O} of the two samples, while σ^2_{Zn-O} in $Zn_{0.80}Co_{0.20}O$ is twice as large as that in $Zn_{0.98}Co_{0.02}O$, reflecting an increasing local structure disorder around Zn with doping.

From analysis of XANES and EXAFS data, the presence of CoO_4 tetrahedra and the changes of the matrix structure as a result of Co doping are well-established, although other structural aspects still need to be understood. Indeed, the observation of different DWs, in particular the occurrence of σ^2_{Co-O} slightly larger than σ^2_{Zn-O} in the low-doping sample, may support the formation of distorted CoO_4 tetrahedra inside the ZnO matrix. However, because of the low-doping level, a small distortion of the ZnO_4 structure is not detectable. On the contrary, detection of similar σ^2_{Co-O} in the two samples indicates that the presence of distorted tetrahedra does not depend on doping; many more CoO_4 tetrahedra are detected in the high Co-doped sample. In addition, the fact that σ^2_{Zn-O} in $Zn_{0.80}Co_{0.20}O$ is twice as large as that in the low-doped sample ($Zn_{0.98}Co_{0.02}O$) addresses the occurrence of distorted ZnO_4 tetrahedra also in the high-doped system, suggesting an important interaction of distorted CoO_4 tetrahedra with the host matrix. Summarizing, because MS calculations show that this system is a substitutional oxide, the doping by Co may act as a "strain defect"[28] and induces the presence of distorted tetrahedra in the ZnO matrix. Interaction with the whole matrix will probably occur over a certain doping concentration that must be identified.

In the mechanism focused on spin−orbit-lattice coupling, the Jahn−Teller-like lattice distortion of the matrix may play an important part in the interplay between magnetic ions. Our investigation actually shows the existence of a distorted lattice structure and addresses a diffusion of the distortion in the matrix versus doping. Within this structural framework, previous investigations[5,29] focusing on the dependence of magnetization on doping could be reanalyzed. Indeed, while at low doping, the lattice distortion is limited to a region around each magnetic ion, and the system exhibits a small magnetization. The same is expected to occur at high doping; if M−O−M (M denotes the magnetic ions) bond chains are formed[5] a superexchange mechanism occurs. As a consequence, within the framework of small local magnetization, only a system characterized by moderate doping concentrations may exhibit the largest magnetization at room temperature.

C. O K-edge XANES. To gain further insight into the doping mechanism and the effect on the oxygen local structure, a comparison of XANES spectra at the O K-edge in $Zn_{1-x}Co_xO$ samples and ZnO is presented in Figure 5a. All spectra were background subtracted and normalized in the energy region from 525 to 556 eV. Five main features can be clearly resolved in the pure ZnO sample and have been labeled from A to E. The features in the energy range of 530−550 eV have been assigned to the O 2p orbitals hybridized with Zn 4s and 4p states.[30] From Figure 5a, we also notice that the curve of $Zn_{0.98}Co_{0.02}O$ is close to that of reference ZnO, while in $Zn_{0.8}Co_{0.2}O$, three significant changes can be observed. Comparison with the ZnO spectra shows at first a broadening of feature A addressing a distorted local coordination environment. Moreover, O 1s XANES of $Zn_{0.8}Co_{0.2}O$ shows a spectral weight shifted to lower energies to the bottom of the conduction band. Finally, the pre-edge peak B' addresses an increase of O 2p holes in the $Zn_{0.8}Co_{0.2}O$ sample. According to the occurrence of bonding−antibonding states, the first local and partial empty state are Co 3d states hybridized with O 2p states, i.e., e_g-t_2 symmetry bands separated by "ligand-field splitting" (ionic crystal field splitting plus hybridization). In the case of a tetrahedral environment, we assigned peak B' to t_2 unoccupied states.

In order to distinguish the scattering contribution from different coordination shells, we performed MS calculations of O K-edge XANES by using different cluster sizes. Data are compared in Figure 5b. For a cluster with oxygen as the central atom, the first shell consists of three Zn and one Co atoms, instead of four Zn atoms as in the ZnO reference compound. Peak B' is well-reproduced by using first shell atoms, and to demonstrate that feature B' is due to cobalt doping, we also calculated ZnO XANES using a five-atom cluster to show the absence of peak B'. Therefore, in a tetrahedral structure in which

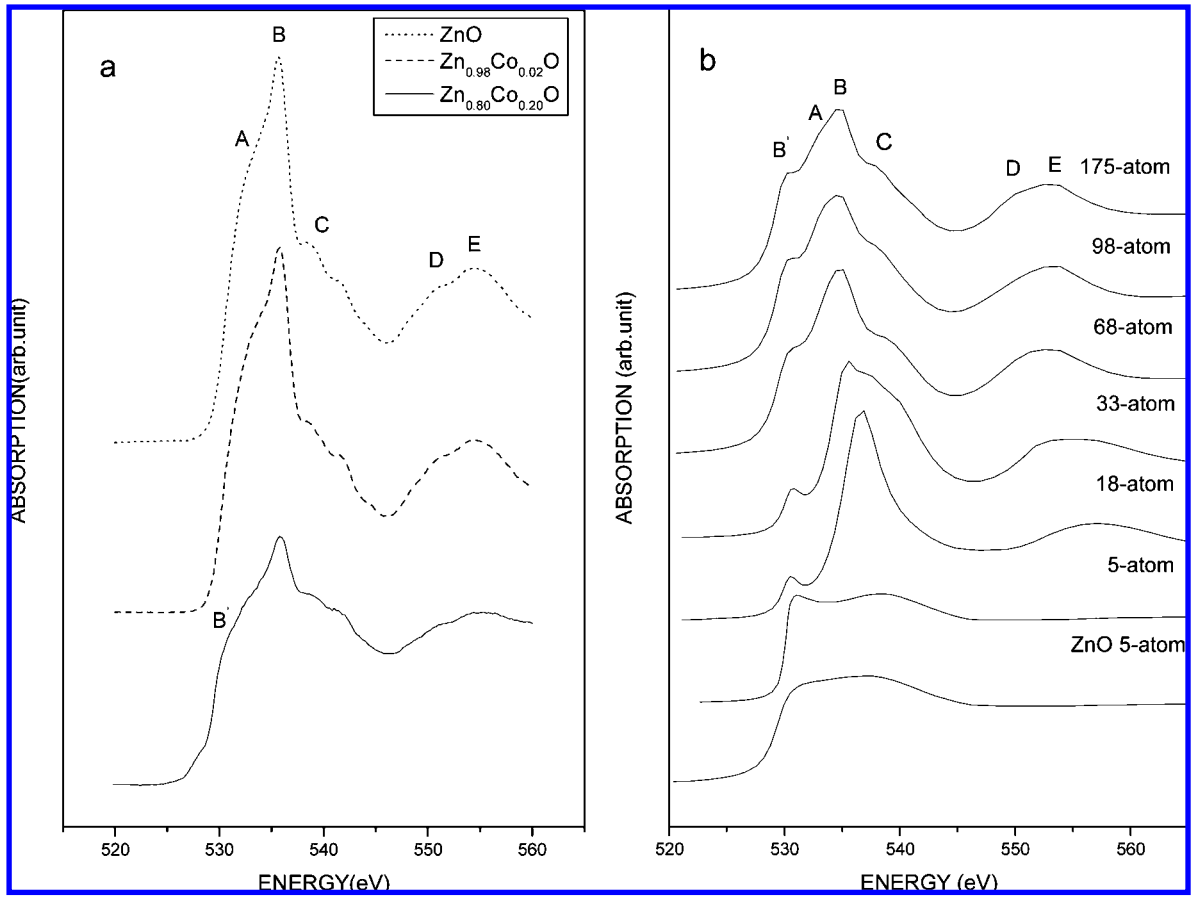

Figure 5. (a) Comparison of the O K-edge XANES spectra of $Zn_{1-x}Co_xO$ ($x = 0$, 0.02, and 0.20) compounds. (b) Comparison of MS calculations at the O K-edge of Co-doped ZnO for different atomic clusters. For comparison, the spectrum of the ZnO system by using a five-atom cluster is also shown.

cobalt atoms replace zinc, feature B' corresponds to a transition to O 2p states hybridized with Co 3d states. From Figure 5b, we notice also that the accurate energy position and intensity are reproduced only in the larger cluster calculations, i.e., we have to take into account higher coordination shells to simulate the real molecular orbital contributions. The 18-atom cluster gives rise to a sharp feature B and partially contributes to features D and E. This cluster well-reproduces feature B, describing the transition to 2p states hybridized with Zn 4sp states demonstrating the contribution of the relatively strong backscattering of O^{2-} ions, actually at the origin of the sharp scattering resonance around the absorber atom. Also, feature C is reproduced by this cluster addressing the main role of single-scattering contributions of oxygen ions within this shell. Peak A is also present in the 68-atom cluster calculation accounting for higher shell contributions. Actually, at O K-edge XANES, the white line peak is mainly determined by the arrangement of the second coordination shell around the absorber. A decrease in the intensity in the $Zn_{0.8}Co_{0.2}O$ spectrum implies a distorted lattice structure in the medium-range order, an effect clearly due to doping. However, MS calculations alone are not able to explain the wide distribution of the O 2p states and the shift of the spectral weight of the $Zn_{0.8}Co_{0.2}O$ spectrum toward low energies. The effect is probably due to a complex hybridization mechanism among cobalt, oxygen, and zinc orbitals, where effect could be clarified only by studying different band structures. To this purpose, we compared partial DOS calculations between pure ZnO and a 25% Co-doped ZnO sample. Calculations are shown in panels a and b of Figure 6 and compared with experimental data. Zn 4s and 4p and O 2p partial DOS for pure ZnO agree very well with previous investigations.[28] In particular, Figure 6a shows the distribution in the conduction band of Zn 4s and 4p states is very narrow with resonance at ~9.1 eV above the Fermi level, which contributes to the observed white line peak. Zn 4s and 4p states are quite close in energy, implying strong hybridization between them. As is well-understood, the energy gap of ZnO is the result of the Zn 4sp and O 2p interaction, which opens a gap between these band states.

To gain more information on the electronic structure in the bottom of the conduction band, we also performed DOS calculations based on DFT. Actually, in our DOS calculations, we do not introduce a core hole when using VASP; thus, calculations return results regarding the ground state of the system. Comparisons between experimental data and theoretical results must be seen mainly in a qualitative way, and we cannot refer to calculations for exact energy positions. Figure 6b shows the comparison between XANES and calculations of the Zn 4s and 4p, O 2p, and Co 3d partial DOS for the $Zn_{0.8}Co_{0.2}O$ sample. These partial DOS are similar to those of ZnO; however, although no additional peaks are detected, differences are also present. Compared to pure ZnO, the distribution of the Zn 4s and 4p partial DOS is wider, and the intensity of the main peak at ~9.1 eV is lower with an overall spectral weight shifted toward the bottom of the conduction band. The behavior is consistent with a white line that is broader and lower in energy, as is observed at the O and Zn *K*-edges in the $Zn_{0.8}Co_{0.2}O$ sample. The Co 3d partial DOS also shows that t_2 unoccupied states are present in the conduction band and mainly contribute to peak B' in Figure 5. The energies of the Co 3d occupied

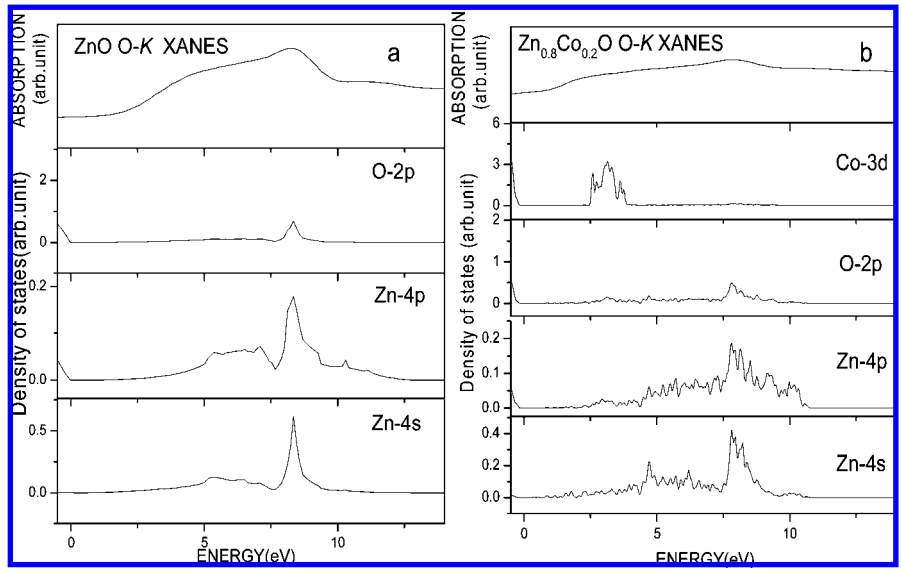

Figure 6. Calculations of the partial density of states for (a) ZnO powders and (b) 25% Co-doped ZnO.

states and Zn 4s and 4p states pinning at the Fermi level are energetically close, addressing the occurrence of strong hybridization. From band calculations, we also stress that the origin of the spectral weight shifts and broad main peak could be affected by complex interplay among Co 3d, Zn 4sp, and O 2p states.

From analysis of O K-edge XANES, we obtain information on the electronic structure of the bottom of the conduction band and recognize changes associated to Co doping, e.g., broadening of certain features, shift of the spectral weight, and a feature originated by hybridization between the Co 3d and O 2p states. By comparison with calculations, two contributions responsible for redistribution of the O 2p empty states have been proposed. The first is due to empty 3d states of dispersed Co atoms inside the ZnO matrix and also to the interaction among Co 3d, Zn 4sp, and O 2p states as evidenced by DOS calculations of the ideal lattice structural model. The second, probably more important, is associated with lattice distortion, which is supported by MS calculations. Indeed, the lattice distortion induces broadening of multiple-scattering contributions and, as a consequence, also of XANES features at the O K-edge.

Conclusions

This work presents results of a systematic XAS investigation performed on Co-doped ZnO samples by studying the local environment around Co, Zn, and O sites. Analysis of metal K-edge XANES showed, in agreement with MS calculations, that the arrangement of the first coordination shell of cobalt is almost not affected by cobalt doping, while at the highest Co concentration, a significant effect on the local structure of Zn atoms is observed, and the behavior is well confirmed by EXAFS analysis.

XANES spectra at the O K-edge and their comparison with MS calculations with different cluster sizes address the presence of a large distortion occurring in the medium-order structure of the highly doped sample. The presence of a distorted lattice structure has been identified, and this effect forming distorted tetrahedra in the ZnO matrix due to Co doping may play a key role similar to a "strain defect".[28] This effect propagates over the whole matrix as a function of doping. By understanding this effect fully, we may possibly have a clearer understanding of previous experimental investigations.[5,29]

From the O K-edge XANES, additional electronic information may be obtained such as hybridization effects caused by Co substitutions. Indeed, because of DOS and MS calculations, two specific contributions caused by the redistribution of O 2p empty states at high doping concentration have been recognized. The first is due to the complex interplay among Co 3d, Zn 4s and 4p, and O 2p states at an increasing Co 3d orbital, while the second, which is much more important in DMS semiconductors, has been associated to a matrix lattice distortion.

Acknowledgment. We sincerely thank A. Marcelli for many helpful discussions. This work was partly supported by National Outstanding Youth Fund (Project 10125523 to Z.W.) and by Knowledge Innovation Program of the Chinese Academy of Sciences (KJCX2-SW-N11).

Supporting Information Available: Parameters of fit of $Zn_{1-x}Co_xO$ when relaxing all parameters (table and figures). This material is available free of charge via the Internet at http://pubs.acs.org.

References and Notes

(1) Ohno, H. *Science* **1998**, *281*, 951.
(2) Wolf, S. A.; Awschalom, D. D.; Buhrman, R. A.; Daughton, J. M.; von Molnar, S.; Roukes, M. L.; Chtchelkanova, A. Y.; Treger, D. M. *Science* **2001**, *294*, 1488.
(3) Kuroda, S.; Nishizawa, N.; Takita, K.; Mitome, M.; Bando, Y.; Osuch, K.; Dietl, T. *Nat. Mater.* **2007**, *6*, 440.
(4) Raebiger, H.; Lany, S.; Zunger, A. *Phys. Rev. Lett.* **2007**, *99*, 167203.
(5) Wang, X. F.; Xu, J. B.; Zhang, B.; Yu, H. G.; Wang, J.; Zhang, X. X.; Yu, J. G.; Li, Q. *Adv. Mater.* **2006**, *18*, 2476.
(6) Griffin, K. A.; Pakhomov, A. B.; Wang, C. M.; Heald, S. M.; Krishnan, K. M. *Phys. Rev. Lett.* **2005**, *94*, 157204.
(7) Quilty, J. W.; Shibata, A.; Son, J. Y.; Takubo, K.; Mizokawa, T.; Toyosaki, H.; Fukumura, T.; Kawasaki, M. *Phys. Rev. Lett.* **2006**, *96*, 027202.
(8) Dietl, T.; Ohno, H.; Matsukura, F.; Cibert, J.; Ferrand, D. *Science* **2000**, *287*, 1019.
(9) Coey, J. M. D.; Venkatesan, M.; Fitzgerald, C. B. *Nat. Mater.* **2005**, *4*, 173.
(10) Dionne, G. F. *J. Appl. Phys.* **2007**, *101*, 09C509.
(11) Yu, Z. G.; He, J.; Xu, S.; Xue, Q.; van't Erve, O. M. J.; Jonker, B. T.; Marcus, M. A.; Yoo, Y. K.; Cheng, S.; Xiang, X.-D. *Phys. Rev. B* **2006**, *74*, 165321.
(12) Li, W.; Kang, Q. Q.; Lin, Z.; Chu, W. S.; Chen, D. L.; Wu, Z. Y.; Yan, Y.; Chen, D. G.; Huang, F. *Appl. Phys. Lett.* **2006**, *89*, 112507.

(13) Martinez-Criado, G.; Segura, A.; Sans, J. A.; Homs, A.; Pellicer-Porres, J.; Susini, J. *Appl. Phys. Lett.* **2006**, *89*, 061906.
(14) Shi, T. F.; Zhu, S. Y.; Sun, Z. H.; Wei, S. Q.; Liu, W. H. *Appl. Phys. Lett.* **2007**, *90*, 102108.
(15) Yan, W.; Sun, Z.; Liu, Q.; Li, Z.; Shi, T.; Wang, F.; Qi, Z.; Zhang, G.; Wei, S.; Zhang, H.; Chen, Z. *Appl. Phys. Lett.* **2007**, *90*, 242509.
(16) Garcia, J.; Blasco, J.; Proietti, M. G.; Benfatto, M. *Phys. Rev. B* **1995**, *52*, 15823.
(17) Yuhas, B. D.; Zitoun, D. O.; Pauzauskie, P. J.; He, R. R.; Yang, P. D. *Angew. Chem., Int. Ed.* **2006**, *45*, 420.
(18) Lee, P. A.; Pendry, J. B. *Phys. Rev. B* **1975**, *11*, 2795.
(19) Natoli, C. R.; Benfatto, M.; Brouder, C.; López, M. F. R.; Foulis, D. L. *Phys. Rev. B* **1990**, *42*, 1944.
(20) Ankudinov, A. L.; Ravel, B.; Rehr, J. J.; Conradson, S. D. *Phys. Rev. B* **1998**, *58*, 7565.
(21) Tyson, T. A.; Hodgson, K. O.; Natoli, C. R.; Benfatto, M. *Phys. Rev. B* **1992**, *46*, 5997.
(22) Newville, M. *J. Synchrotron Radiat.* **2001**, *8*, 322.
(23) Kresse, G.; Hafner, J. *Phys. Rev. B* **1993**, *47*, 558.
(24) Sawniczak-Jabłonska, K.; Iwanowski, R. J.; Gołacki, Z.; Traverse, A.; Pizzini, S.; Fontaine, A.; Winter, I.; Hormes, J. *Phys. Rev. B* **1996**, *53*, 1119.
(25) Wu, Z. Y.; Xian, D. C.; Hu, T. D.; Xie, Y. N.; Tao, Y.; Natoli, C. R.; Paris, E.; Marcelli, A. *Phys. Rev. B* **2004**, *70*, 033104.
(26) Wu, Z. Y.; Ouvrard, G.; Gressier, P.; Natoli, C. R. *Phys. Rev. B* **1997**, *55*, 10382.
(27) Wu, Z.; Xian, D. C.; Natoli, C. R.; Marcelli, A.; Paris, E.; Mottana, A. *Appl. Phys. Lett.* **2001**, *79*, 1918.
(28) Eshelby, J. D. *Proc. R. Soc. London, Ser. A* **1957**, *241*, 376.
(29) Chiou, J. W.; Tsai, H. M.; Pao, C. W.; Kumar, K. P. K.; Chen, J. H.; Ling, D. C.; Chien, F. Z.; Pong, W. F.; Tsai, M. H.; Wu, J. J.; Yang, M. H.; Liu, S. C.; Hong, I. H.; Chen, C. H.; Lin, H. J.; Lee, J. F. *Appl. Phys. Lett.* **2007**, *90*, 062103.
(30) Dong, C. L.; Persson, C.; Vayssieres, L.; Augustsson, A.; Schmitt, T.; Mattesini, M.; Ahuja, R.; Chang, C. L.; Guo, J. H. *Phys. Rev. B* **2004**, *70*, 195325.

JP807459S